J. Quant. Spectrosc. Radiat. Transfer, Vol. 19, pp. 69–81. Pergamon Press 1978. Printed in Great Britain

SOME NEW TRANSITION PROBABILITIES FOR MERCURY I†

EARL R. MOSBURG, JR. and MARK D. WILKE

Laser Physics Section, National Bureau of Standards, Boulder, CO 80302, U.S.A.

(*Received* 8 *April* 1977)

Abstract—Detailed studies of a pure mercury positive column have allowed us to determine the densities and effective temperatures which characterize the discharge. From this knowledge of the discharge conditions, a series of transition probabilities is derived for 70 lines in the neutral mercury spectrum in the wavelength range 238–1530 nm, including many lines for which transition probabilities have not previously been published.

1. INTRODUCTION

AT THE present time, the literature on the transition probabilities of neutral mercury contains a diversity of values.[1–6] In connection with experiments we have carried out at this laboratory on a constricted positive column discharge in pure mercury vapor,[7] for which it was necessary to characterize the discharge thoroughly, we have found that the atomic levels were in collisional equilibrium at effective electron temperatures between 0.40 and 0.45 eV. The experimental procedures and analysis used to reach this conclusion are summarized in Section 2.

In this paper, we have analyzed our relative spectral emission intensity data, from 220 to 1600 nm, to obtain a set of absolute transition probabilities for 70 lines in the Hg(I) spectrum. To obtain these absolute values, we have used some recently published measurements of atomic radiation lifetimes[8–11] (see Table 1). In cases where the relative transition probabilities were measured for all lines originating on a common upper level, we have renormalized these values so that their sum is equal to the reciprocal of the radiative lifetime of this level, thus obtaining a series of absolute values. The absolute transition probabilities of other lines in the same spectral scan can then be calculated. The final result of our efforts is the list of oscillator strengths or A-values given in Table 3, which includes many transitions for which such values have not previously been reported.

2. APPARATUS AND MEASUREMENTS

The basic arrangement of the experimental discharge tubes is shown in Fig. 1. The tubes were mainly of quartz with glass to metal seals used to form hollow electrodes. The observing region consisted of a quartz tube of square cross section measuring 10 mm inside. The discharge region was contained in an upper oven maintained at a temperature of 600–650 K and the mercury pressure was controlled by a lower oven temperature surrounding the side arm and its reservoir of liquid mercury. The lower oven temperature was maintained to within ±1°C, corresponding to an error in the atomic gas density, N, of ±3%. This arrangement, as well as the techniques used to obtain a very pure mercury filling, have previously been described in detail.[12] At the gas densities of major interest in this paper, $N = 0.75 \times 10^{18}$ to 10^{19} cm^{-3} (approx. 60–675 torr), the discharge was a highly constricted positive column. Steady discharge currents from 30 to 100 mA were used. Our discharge conditions are distinguished primarily by the low discharge currents we used, which were 100–1000 times lower than those of the arc discharges more commonly used in determining transition probabilities. Largely because of this difference, we obtain a rich Hg(I) spectrum without producing any appreciable ion spectrum. Two probes were inserted 10 cm apart along the tube axis in order to allow measurement of the axial electric field, E, so that E/N could be calculated. For one set of data, as a check on these potential measurements, the resulting value of the axial field was multiplied by the total

†Based on work supported in part by ERDA Contract No. E (49-1)-3800.

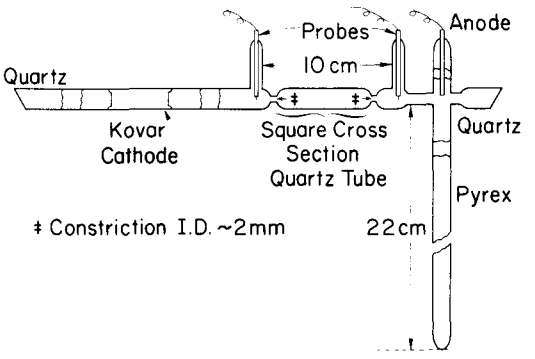

Fig. 1. Diagram of the mercury discharge tube.

Table 1. Lifetimes of mercury levels.

Upper Level		Measured Lifetime	Ref.	Average of lifetime measurements	Corresponding A_{tot}
Designation	Energy [cm^{-1}]	[nsec]		[nsec]	[10^8 sec^{-1}]
7^3S_1	62350	8.4±0.4 8.2±0.2	c d	8.3	1.20
7^1S_0	63928	31.0±0.5 30.3±0.9	a b	30.7	0.326
6^1D_2 6^3D	71333 71396	10.9±0.3 10.8±0.2	b a	10.85	0.922
8^1S_0	74405	84.0±2.0 63.2±4.8	a b	73.6	0.136
7^1D_2	77064	38.5±0.5 40.5±1.5	a b	39.5	0.253
9^1S_0	78404	142±8	b		0.070
8^1D_2	79661	126±7	b		0.079
10^1P_1	81154	51.0±4	a		0.196

Ref: a. G. C. King, A. Adams and D. Cvejanovic, J. Phys. B 8, 365 (1975) (method: electron-photon coincidence).

b. R. Wallenstein, private communication (method: two-photon laser excitation).

c. C. Camhy-Val, A. M. Dumont, M. Dreux and R. Vitry, Phys. Lett. 32A, 233 (1970) (method: correlated photons in cascade).

d. R. A. Holt and F. M. Pipkin, Phys. Rev. A 9, 581 (1974) (method: cascade coincidence).

discharge length and compared with the voltage drop across the discharge tube. The difference indicated a cathode fall of about 275 to 300 V, roughly in agreement with the cathode fall for a normal glow discharge. The neutral gas density, N, was determined from the upper and lower oven temperatures using the mercury vapor-pressure curves with a correction for the gas heating due to the measured electrical power per unit length of discharge, $P(\mathrm{Wcm}^{-1})$.

The u.v. and visible spectrum was observed using a 33 cm Czerny–Turner spectrometer and an electrically cooled 9558QA S-20 photomultiplier. The relative response function of the spectrometer-detector system was determined using a calibrated tungsten iodide lamp, and subsequently the absolute response function was measured using a calibrated deuterium lamp which also extended the calibration to 180 nm. When the relative calibration was joined to the absolute one at $\lambda = 298$ nm, the two curves were in very good agreement (±1.5%) over the range from 285 to 305 nm and within 13% to $\lambda = 400$ nm, which is the limit of the calibrated range of the deuterium lamp.

The observed u.v. and visible emission spectrum, after correction for the instrumental response function, is shown in Fig. 2(a). It connsists of several dozen Hg(I) lines and the broad molecular band at 335 nm due to the transition from the 1_u excimer to the O_g^+ dissociative dimer ground state [see Refs. (7), (13)]. The ratio of the total photon emission rate in the atomic lines, including i.r. lines to $\lambda = 1.53\ \mu$m, to the emission rate in the 335 nm band is approx. 25. The spectrometer was nitrogen-flushed in order to extend the measurements to the 185 nm resonance line. All of the brighter lines are due to Hg(I), with the exception of the prominent 194.2 nm Hg(II) transition.

The i.r. spectrum was measured using a 0.8 meter Fastie–Ebert spectrometer of NBS design with a 600 line/mm grating blazed at 1 μm. Two types of detectors were utilized. In the wavelength region of 600–1220 nm, we used a specially selected 6911 photomultiplier having S-1 response, cooled by liquid nitrogen boil-off to a temperature of −35°C. For the spectral region from 650 to 1680 nm, a room-temperature germanium diode detector was employed. A section of this spectrum is shown in Fig. 2(b). In both cases, the response function of the spectrometer-detector system was determined using a calibrated tungsten iodide lamp.

In order to determine the radial dependence of some of the spectral features, the light from the discharge column was passed through a scanning mirror geometry (Fig. 3) and was focused with a magnification between three and four onto a horizontal slit just in front of the spectrometer. This allowed a measurement of the spacial distribution of the emitted light from which the diameters of the light-emitting regions could be determined. The procedure is described more fully in Ref. (7). Generally, a horizontal slit width of 0.5 mm was used, resulting in a radial resolution of 0.2 mm or better. Most of the atomic lines, except the resonance lines, showed similar, very narrow spacial profiles, having nearly equal full widths at half maximum (FWHM). Once the diameter of the conducting column was established, the electron density, n_e, was then estimated from the current density using $J = n_e e v_d$, where the drift velocity v_d was

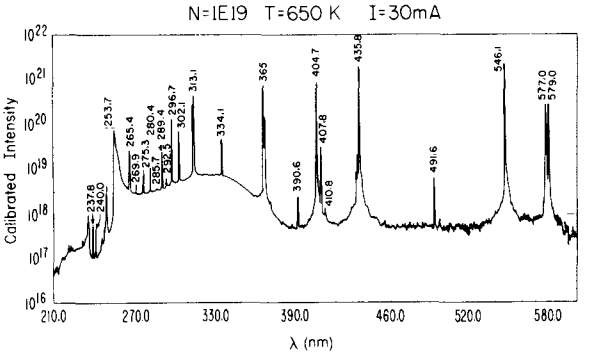

Fig. 2(a). Emission spectrum of the mercury discharge for a gas density of $1 \times 10^{19}\ cm^{-3}$ and a discharge current of 30 mA. Correction has been made for the spectral response function of the spectrometer and photomultiplier.

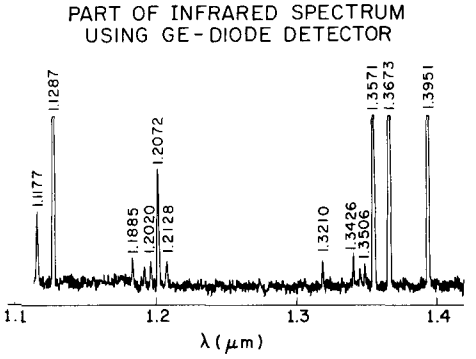

Fig. 2(b). Emission spectrum of the mercury discharge for a current of 30 mA and a gas density of $1.6 \times 10^{18}\ cm^{-3}$ in the i.r. region using a germanium diode detector. This is the raw spectrum, prior to correction for the instrumental response function.

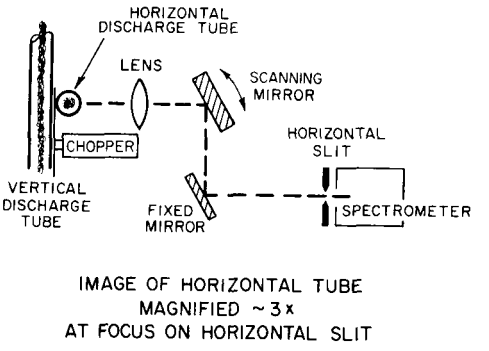

Fig. 3. Diagram showing the optical scanning system used to obtain spacially resolved emission and absorption profiles.

obtained from measured E/N. Details of this procedure are given in Ref. (7). The electron-density values were generally in the range 10^{14} to $10^{15}\,cm^{-3}$. Data from E/N measurements do not allow a good determination of the characteristic electron temperature. Roughly, values in the range 0.4 to 0.7 eV would be expected. Langmuir-probe measurements, made at the edge of the discharge operating at 30 mA and $N = 1.7 \times 10^{18}\,cm^{-3}$, resulted in nearly exponential curves corresponding to electron temperatures of 0.4–0.6 eV. However, the best technique for establishing the effective electron temperature is, as described below, the comparison of relative line-emission intensities since the whole manifold of atomic levels seems to be nearly in Maxwell–Boltzmann equilibrium.

Using the discharge at 30 mA and a gas density $N = 1 \times 10^{18}\,cm^{-3}$, the absolute emission intensities of several atomic lines originating on 7^3S_1 and 8^1S_0 levels, for which reasonably reliable radiative lifetime values are now available (see Table 1), lead to the excited atom densities shown in Fig. 4. The procedures will be discussed in Section 3. In addition, estimates of the densities of the 6^3P_0, 6^3P_1, 6^3P_2, and 6^1P_1 levels were obtained by measuring the optical absorption on a series of atomic lines, and using transition probabilities from Refs. (1) and (2). The scanning-mirror geometry (Fig. 3) was used for these measurements and a second mercury discharge tube, similar to the main horizontal one, was placed in the same oven with its discharge column vertical and directly behind the main tube as a line source for the absorption measurements [see Ref. (7) for details].

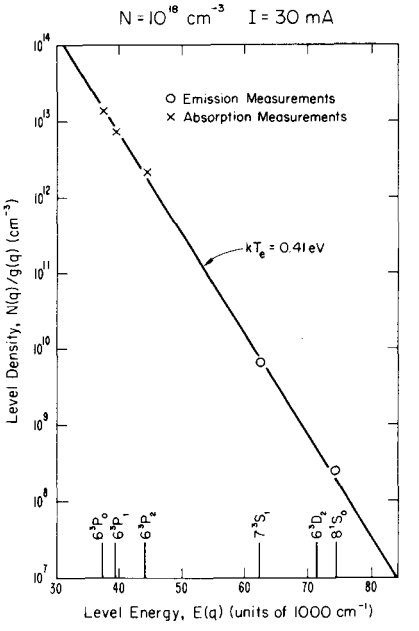

Fig. 4. Relation between the energy of various levels and the weighted population densities of these levels for a discharge current of 30 mA and a gas density of $N = 1 \times 10^{18}\,cm^{-3}$.

The resulting calculated absorber densities, divided by their weighting functions, are shown in Fig. 4. We now see that not only the densities of the 7^3S_1 and 8^1S_0 levels from absolute emission measurements, but also the densities of the 6^3P_0, 6^3P_1 and 6^3P_2 levels determined from the absorption measurements, are close to collisional equilibrium. The line of best fit shown in Fig. 4 ($kT_e = 0.41$ eV) corresponds to a value of n_e between 1.5 and 1.7×10^{14} cm^{-3}, which compares rather favorably with the value of $n_e = 0.8 \times 10^{14}$ cm^{-3} from the E/N measurements. This result provides strong evidence that the constricted mercury column under study is in Maxwell–Boltzmann equilibrium all the way to the ground state. A comparison of estimated electron collision rates and other reaction rates in the particle-balance equations for excited states does not contradict this.

3. DETERMINATION OF THE TRANSITION PROBABILITIES

The volume emission rate of radiation at a given spectral frequency, ν, within a line of wavelength λ, is the product $A_\lambda \alpha(\nu) N_u(y)$, where $N_u(y)$ is the local number density (cm^{-3}) of the upper, radiating level as a function of position, y, along the line of sight, A_λ is the total transition probability (sec^{-1}) of the particular line being considered, and $\alpha(\nu)$ is the normalized spectral emission profile, $\int \alpha(\nu)\, d\nu = 1$. The resulting signal strength at the detector, after correction for the response function of the spectrometer and detector, I_λ, is proportional to the emission rate integrated both along the detector line of sight and over the spectral profile and modified by any self-absorption. The fraction of the emitted light which reaches the detector after traversing the medium from position y is $\exp(-\sigma\beta(\nu)\int_y^\infty N_l(y)\, dy$ is the number density of atoms in the lower level as a function of position, y, along the line of sight, σ is the absorption cross section per atom at the line center (σ is independent of y under our experimental conditions), and $\beta(\nu)$ is the line profile of the absorption normalized to unity at the line center, $\beta(\nu_0) = 1$. The total net light at the detector, after integration both over the spectral profile and over the full line of sight of the detector ($y = 0$ at the center of the discharge), is then given by

$$I_\lambda = \text{const}\, A_\lambda \int_{-\infty}^{+\infty} N_u(y) \left[\int_{-\infty}^{+\infty} \alpha(\nu) \exp\left(-\beta(\nu)\sigma \int_y^\infty N_l(y) dy \right) d\nu \right] dy. \tag{1}$$

The corresponding value without absorption, obtained by setting $\sigma = 0$ in eqn (1), is

$$I_{\lambda 0} = \text{const}\, A_\lambda \int_{-\infty}^{+\infty} N_u(y) \left[\int_{-\infty}^{+\infty} \alpha(\nu)\, d\nu \right] dy = \text{const}\, A_\lambda \int_{-\infty}^{+\infty} N_u(y)\, dy. \tag{2}$$

Since the self-absorption in a single discharge tube, A_S, is defined as one minus the ratio of the light actually radiated from the tube to the light which would be radiated in the absence of atomic absorption, we can then write

$$I_\lambda = (1 - A_S)\, I_{\lambda 0}. \tag{3}$$

Because the central regions of the spacial density profiles, $N_u(y)$, can be fit quite well by gaussian functions, we replace the integral in eqn (2) by $N_u(0)\Delta_u$ where Δ_u is the spacial width (FWHM) and $N_u(0)$ is the density on the axis of the discharge,

$$\int_{-\infty}^{+\infty} N_u(y)\, dy = N_u(0) \frac{\Delta_u}{\sqrt{(\ln 2)}} \int_0^\infty e^{-t^2}\, dt = 1.06\, N_u(0)\Delta_u. \tag{4}$$

By using eqns (2) and (4) in eqn (3), the calibrated detector signal strength, I_λ, can be expressed as

$$I_\lambda = \text{const}\,(1 - A_S)\, \Delta_u\, A_\lambda\, N_u(0). \tag{5}$$

We immediately apply the self absorption and emission width corrections to I_λ, defining a new quantity, the corrected signal strength,

$$C_\lambda \equiv \frac{I_\lambda}{(1 - A_s)\Delta_u} = \text{const}\, A_\lambda\, N_u(0). \tag{6}$$

The fractional absorption, A_f, measured by the two-source method mentioned in Section 2 and discussed more fully in Ref. (7) can be related to the self-absorption, A_s, in the manner detailed in the Appendix. Since the photon path thru the absorbing medium is, on the average, half as long for self-absorption as for the two-tube fractional absorption, we expect that $A_s \approx \frac{1}{2} A_F$ when A_F is very small. It turns out (see Table A1) that even when $A_F \approx 0.50$ (approximately the maximum value observed), A_s/A_F has risen only to ≈ 0.6.

Spacial emission and absorption profiles were measured for the 404.7, 435.8 and 546.1 nm lines and for a few others. Since the measured spacial widths, Δ_u, were very similar, and because of the large number of atomic lines involved, such spacial profiles were not measured for the majority of the lines. The fractional absorption of lines in the region 205–410 nm was, however, measured using spectral scans under the appropriate conditions for the two-source method [see Ref. (7) Table A1]. This procedure allowed us to determine rapidly the absorption of many lines and to recognize quickly those few having appreciable self-absorption corrections. In the i.r., since most transitions originate on higher-lying levels for which the atomic density is necessarily much lower, the self-absorptions are generally much smaller. Therefore, for transitions with $\lambda > 600$ nm, the self-absorption corrections were neglected at first. Once the A-values were determined, the expected absorptions of the brighter lines (those with larger A-values) were calculated to see if appreciable corrections were needed. In all cases, these calculated absorptions were very small.

In order to use eqn (6) to obtain A_λ, we must know $N_u(0)$. Since this is generally not accessible to direct measurements, we must use the argument of collisional equilibrium between atomic levels at the electron temperature, as discussed in Section 2 which allows us to write $N_u(0)/g_u = N \exp(-E_u/kT_e)$, where $g_u = 2J + 1$ is the statistical weight of the radiating level and E_u is its energy. Equation (6) then becomes

$$C_\lambda = \text{const}\, A_\lambda N g_u \exp(-E_u/kT_e). \tag{7}$$

Using absolute photon counting in order to determine the proportionality constant in eqn (7), we could in principal obtain A_λ. However, for a fixed fractional error in kT_e, the fractional error in the transition probabilities would be very large because $E_u \gg kT_e$, as we discuss later [see eqn (12)].

Rather than using absolute photon-counting techniques, we have therefore chosen to normalize to a reference line for which the A-value, represented by A_r, is known and which originates on a level close in energy to the levels radiating the lines of unknown A-value. We therefore take the ratio of eqn (7) written for the unknown A-value, A_x, to the same equation for A_r, and solve for A_x in the form

$$A_x = \left[\frac{A_r g_r}{C_r}\right] \frac{C_x}{g_x} \exp\left(\frac{E_x - E_r}{kT_e}\right). \tag{8}$$

As our primary reference for the visible and u.v. spectrum, we have used the total transition probability, $A_{\text{tot}} = \sum_i A(\lambda_i)$, for all four lines radiating from the 7^3S^1 level. These lines occur at $\lambda = 404.7$, 435.8, 546.1 and 1207.2 nm.

The total probability, A_{tot}, is just the reciprocal of the radiative lifetime, τ, of the upper level. Such lifetimes have recently been measured for the 7^3S_1 and other levels, using reliable methods which avoid the errors due to cascading and other effects. A series of such lifetime values is given in Table 1. Summing eqn (7) over the series of four lines, we obtain

$$C_{\text{tot}} = \sum_{i=1}^{4} C_i = \text{const}\, A_{\text{tot}} N g_u \exp(-E_u/kT_e). \tag{9}$$

The only i.r. transition radiating from the 7^3S_1 level, 1207.2 nm, contributes less than 0.5% to the total A-value. Taking the ratio of eqn (7) written for the unknown, A_x, to eqn (9), we again obtain eqn (8), where now A_{tot} and C_{tot} are used in place of A_r and C_r. The transition probabilities of the four constituent lines are then readily determined using eqn (8). The average

A-values determined in this manner from 8 sets of data at four different gas densities and two different discharge currents are given in Table 2, along with the statistical standard deviations. For comparison, we have listed a few of the A-values from previous papers. Although most of the A-values reported in Ref. (4) are in error by very large factors, the values we calculated by renormalizing to obtain the correct 7^3S_1 lifetime are in reasonable agreement with those of other experiments. This renormalization seems, however, to be valid only for lines originating on the 7^3S_1 and 7^1S_0 levels. For other lines, the disagreement of both the renormalized and non-renormalized values from Ref. (1) is so large that we have not included them in Table 3. The average A-value for the 404.7 nm line was, in turn, used as the reference for the spectral scans in the u.v. and visible where the other lines originating on the 7^3S_1 level were not measured. The transition probabilities of other lines, A_x, were then determined, again by means of eqn (8), and are listed in Table 3.

For a calibration of the i.r. spectra, we used as a reference the total transition probability for the two lines 1014.0 and 407.8 nm, which together account for the radiative lifetime of the 7^1S_0 level (see Table 1). Our measured line intensities show that the intercombination line, 407.8 nm, contributes only about 15% to the total transition probability of this level. In a manner similar to that used for the u.v. and visible region, we then establish the transition probability of the 1014.0 nm line as a reference in the i.r. region. The values for other i.r. lines, determined using eqn (8) as for the u.v. and visible region, are also listed in Table 3.

Where several upper levels are responsible for the observed emission, the statistical weight factors also differ and must be included within the summation so that eqn (6) becomes

$$\sum C(\lambda_i) = \text{const} \sum_i A(\lambda_i) N_i = \text{const}\, A_x \sum_i N_i. \tag{10}$$

This equation defines $A_x \equiv \sum_i A(\lambda_i) N_i / \sum_i N_i$. Expanding $\sum_i N_i = N \sum_i (2J_i + 1) \exp(-E_i/kT_e)$ and removing the exponential factor from the summation since the upper levels are only very slightly separated in energy, we obtain

$$C_{x\,\text{tot}} \equiv \sum_i C(\lambda_i) = \text{const}\, A_x N \exp(-E_x/kT_e) \sum_i (2J_i + 1). \tag{11}$$

Table 2. The transition probability in units of 10^8 sec^{-1} for transitions from the reference levels.

λ_{nm}	Lower Level	A-Values (this paper) [10^8 sec^{-1}]	NBS Mono. 53 (Ref. 4) as pub.	NBS Mono. 53 (Ref. 4) renormalized	Jean et al. (Ref. 1)	Pilz & Seehawer (Ref. 2)
		Upper level 7^3S_1 (62350), $g_u = 3$, $1/\tau = \Sigma A = 1.205$				
404.7	6^3P_0	0.186±0.005*	12.0	0.21	0.24	0.17
435.8	6^3P_1	0.424±0.009*	28.7	0.50	0.49	0.43
546.1	6^3P_2	0.592±0.009*	28.7	0.50	0.52	0.62
1207.2	6^1P_1	0.003±0.001		~0		
		ΣA = 1.205	69.34	1.21		
		Upper level 7^1S_0 (63928), $g_u = 1$, $1/\tau = \Sigma A = 0.326$				
407.8	6^3P_1	0.043	2.6	0.045		
1014.0	6^1P_1	0.283				
		ΣA = 0.326				
		Upper level 8^1S_0 (74405), $g_u = 1$, $1/\tau = \Sigma A = 0.136$				
285.7	6^3P_1	0.0111				
491.6	6^1P_1	0.127				0.048
		ΣA = 0.1381				

*Standard deviation for eight independent measurements at four different gas densities and two different discharge currents.

Table 3. Values of $g_x A_x$ in units of 10^8 sec^{-1}.

λ_{nm}	Level Designations		E_u	2J+1	This Experiment					Previous Work
					S-20 PMT		S-1 PMT	Ge-diode	Est.	
	Upper	Lower	cm^{-1}	[Σ(2J+1)]	Ref 7^3S_1	Ref 8^1S_0	Ref 7^1S_0	Ref 7^1S_0	Error ±%*	
237.8	8^3D_1	6^3P_0	79679	3	0.09	0.08			34,23	
240.0	$9^3D_{1,2}$ 9^1D_2	6^3P_1	81071		0.13	0.11			39,26	
264.0	$10^3D_{1,2,3}$ 10^1D_2	6^3P_2	81906		0.30	0.27			39,26	
265.4	$7^3D_{1,2}$ 7^1D_2	6^3P_1	77086	[13]	2.02	1.83			29,21	
269.9	$9^3D_{1,2,3}$ 9^1D_2	6^3P_2	81073		0.63	0.57			36,24	
275.3	8^3S_1	6^3P_0	73961	3	0.18	0.16			24,21	0.11^a
280.4	$8^3D_{1,2,3}$ 8^1D_2	6^3P_2	79683		1.41	1.27			34,23	
285.7	8^1S_0	6^3P_1	74405	1	0.013	0.011			25,21	
289.4	8^3S_1	6^3P_1	73961	3	0.49	0.44			24,21	0.33^a
292.5	9^3S_1	6^3P_2	78216	3	0.24	0.21			31,22	0.20^a
296.7	6^3D_1	6^3P_0	71336	3	1.43	1.24			20,22	3.0^b 2.94^c 3.0^d
302.1	$7^3D_{1,2,3}$ 7^1D_2	6^3P_2	77097		4.64	4.20			29,21	
312.6	6^3D_2	6^3P_1	71396	5	2.66	2.41			20,22	3.1^b 3.5^c 16.5^e
313.2	6^3D_1 6^1D_2	6^3P_1	71336	[8]	4.31	3.90			20,22	4.92^b 5.35^c 8.0^d
334.1	8^3S_1	6^3P_2	73961	3	0.84	0.76			24,21	0.48^a
365.2	$6^3D_{2,3}$	6^3P_2	71410		9.41	8.53			20,22	10.6^b 10.4^d
366.3	6^3D_1 6^1D_2	6^3P_2	71330							
390.6	8^1D_2 $8^3D_{1,2}$	6^1P_1	79677		0.33	0.30			34,23	0.17^c
404.7	7^3S_1	6^3P_0	62350	3	0.558R	0.51			5,30	0.72^b 0.51^c 0.63^f 0.41^a 1.56^e
407.8	7^1S_0	6^3P_1	63928	1	0.043	0.038			5,28	0.045^f 0.13^e
410.8	9^1S_0	6^1P_1	78404	1	0.031	0.028			31,22	
433.9	7^3D_2	6^1P_1	77108	5	0.42	0.38			29,21	0.15^c
434.4	7^1D_2 7^3D_1	6^1P_1	77075		1.34	1.22			29,21	0.48^c
435.8	7^3S_1	6^3P_1	62350	3	1.27	1.11			5,30	1.47^b 1.29^c 1.50^f 1.16^a 3.6^e
491.6	8^1S_0	6^1P_1	74405	1	0.14	0.127R			25,15	0.048^c
546.1	7^3S_1	6^3P_2	62350	3	1.77	1.57			5,30	1.56^b 1.86^c 1.50^f 1.57^a 3.3^e
577.0	6^3D_2	6^1P_1	71396	5	3.26	2.92	2.90		20,22,20	1.35^b 1.8^c 0.80^e

Table 3. (*Contd*).

λ_{nm}	Level Designations		E_u	2J+1	This Experiment					Previous Work
					S-20 PMT		S-1 PMT	Ge-diode	Est.	
	Upper	Lower	cm^{-1}	[Σ(2J+1)]	Ref 7^3S_1	Ref 8^1S_0	Ref 7^1S_0	Ref 7^1S_0	Error ±%*	
579.0	6^1D_2 6^3D_1	6^1P_1	71335		3.16	2.86	2.29		20,22,20	1.0[b] 1.66[c]
607.2	6p' $^1P_1$	7^3S_1	78813	3			0.003		86	
623.4	9^1P_1	7^1S_0	79964	3			0.016		31	
671.6	6p' $^1P_1$	7^1S_0	78813	3			0.013		27	
690.7	8^3P_2	7^3S_1	76824	5		0.16	0.12		30,20	
708.7	8^3P_1 8^3P_0	7^3S_1	76457	[4]			0.037		20	
767.7	$10^3D_{1,2,3}$ 10^1D_2	6p' $^3P_2$	81906				0.010		50	
772.9	8^1P_1	7^1S_0	76863	3			0.029		22	
782.	$11^3D_{1,2}$ 11^1D_2	7^3P_1	82442				0.010		58	
816.7	$10^3D_{1,2}$ 10^1D_2	7^3P_1	81900				0.017		37	
820.0	$9^3D_{1,2,3}$ 9^1D_2	6p' $^3P_2$	81080				0.018		32	
865.2	9^3D_1	7^3P_0	81071	3			0.014		39	
875.7	9^3D 10^3F	7^3P_1	81075				0.042		30	
889.5	$11^3D_{1,2,3}$	7^3P_2	82445				0.025		41	
906.8	$9^{3,1}F$	6^3D_2	82455				0.022		44	
925.	$8^3D_{1,2,3}$ 8^1D_2	6p' $^3P_2$	79690				0.044		26	
933.8	$10^3D_{1,2,3}$ 10^1S_0	$7^3P_{1,2}$	80366				0.020		40	
944.	$8^{1,3}F_{2,3}$	6^1D_2 $6^3D_{1,2}$	81924				0.096		32	
949.5	$8^3F_{2,3}$ 8^1F_3	6^3D_2	81924				0.029		36	
952.6	$8^3F_{2,3,4}$ 8^1F_3	6^3D_3	81925				0.036		33	
983.8	8^3D_1	7^3P_0	79679	3			0.035		28	
996.89	8^3D_2	7^3P_1	79690	5			0.063		26	
999.84	8^1D_2	7^3P_1	79661	5			0.024		31	
1014.0	7^1S_0	6^1P_1	63928	1			0.283R	0.283R	6,6	0.29[e]
1023.	7^3F	6^1D_1 6^3D_1	81106				0.082		28	
1030.	$7^3F_{2,3,4}$ 7^1F	6^3D_2	81100				0.072		30	
1033.	7^3F 7^1F	6^3D_3	81100				0.097		28	

Table 3. (*Contd*).

λ_{nm}	Level Designations		E_u	2J+1	This Experiment				Previous Work
					S-20 PMT		S-1 PMT	Ge-diode	Est.	
	Upper	Lower	cm^{-1}	[Σ(2J+1)]	Ref 7^3S_1	Ref 8^1S_0	Ref 7^1S_0	Ref 7^1S_0	Error ±%*	
1071.6	9^3S_1 $9^3F_{2,3,4}$	$6p'^3P_2$ $6p'^3D_3$	78216				0.027		34	
1117.7	7^1P_1	7^3S_1	71295	3				0.11	30	0.15[e]
1128.7	7^3P_2	7^3S_1	71208	5				1.78	13	0.99[d] 2.2[e]
1188	$6^3F_{2,3}$ 6^1F_3	6^3D_1 6^1D_2	79745					0.59	45	
1197	$6^3F_{2,3,4}$	6^3D_2	79745					0.23	61	
1202.	6^3F	6^3D_3	79745					0.47	48	
1207.2	7^3S_1	6^1P_1	79613	3			0.007	0.012	27,36	<0.03[c] 0.006[e]
1212.8	7^3D_3	$6p'^3P_2$	77130	7				0.16	50	
1321.0	7^3D_1	7^3P_0	77085	3				0.18	46	
1342.6	7^3D_2	7^3P_1	77108	5				0.25	42	
1346.8	7^3D_1	7^3P_1	77085	3				0.095	65	
1350.6	7^1D_2	7^3P_1	77064	5				0.15	50	
1357.1	7^1P_1	7^1S_0	71295	3				1.66	16	0.54[e]
1367.3	7^3P_1	7^3S_1	69662	3				1.27	11	0.43[d] 0.54[e]
1395.1	7^3P_0	7^3S_1	69517	1				0.52	16	0.13[d] 0.23[e]
1529.5	$6p'^3P_2$	7^3S_1	68887	5				0.56	15	

*Estimated errors are tabulated in respective order for entries to the left

[a]Gruzdev, Opt. Spectrosc. 22 89 (1967) (theoretical calculation)

[b]Jean, Martin, Barrat and Cojan, Compt. Rend. 264 1709 (1967)

[c]Pilz and Seehawer, Proceedings of 12th Conf. on Phen. in Ion Gases Eindhoven Part 1 p. 146 North-Holland 1975

[d]Platz, J. Physique 32 773 (1971)

[e]Anderson, Lee and Lin, Phys. Rev. 159 31 (1967) (theoretical calculation)

[f]Corliss and Bozman, NBS Monograph 53 (1962) (renormalized)

R indicates a line was used as a reference for determining absolute A-values (see text)

Taking the ratio to the reference line as before, we again obtain an expression of the form of eqn (8), where now C_x is replaced by $C_{x\,\mathrm{tot}}$ and $g_x = 2J+1$ by $g_x = \sum_i (2J_i+1)$. Because of possible ambiguities in some cases as to which upper levels contribute "significantly" to a particular observed line, we have listed only the products $g_x A_x$ in Table 3. Where such ambiguities occur, we have not listed values for $\Sigma(2J+1)$.

A major contribution to the error for the majority of A-values listed in Table 3 is due to the uncertainty in the electron temperature through the Boltzmann factor in eqn (8). An estimate of the error can be obtained by taking the derivative of this equation with respect to kT_e. The fractional error in A_x is related to the fractional error in kT_e by the expression

$$\frac{\Delta A_x}{A_x} = \frac{E_x - E_r}{kT_e}\frac{\Delta kT_e}{kT_e}. \tag{12}$$

A given fractional error in kT_e will therefore produce a much larger fractional error in A_x when $E_x - E_r \gg kT_e$. Thus, in our data where $\Delta kT_e/kT_e$ is $\pm \sim 3$–5%, contributions to the fractional errors in A_x as large as ±18–30% can result for lines originating on the higher lying levels when the 7^3S_1 level ($E_u = 62350\ \mathrm{cm}^{-1}$) is used as a reference.

One way to improve the accuracy in this case would be to find a new reference line originating on a level lying higher than the 7^3S_1 level, whose lifetime has also been determined independently. The 491.6 nm transition, originating on the 8^1S_0 ($74405\ \mathrm{cm}^{-1}$) level, provides such a possibility. Since the other line radiating from this level is the intercombination transition at 285.7 nm ($8^1S_0 \rightarrow 6^3P_1$), which provides only 8% of the total transition probability (see Table 2), we can accurately determine the A-value for the 491.6 nm line from the measured radiative lifetime of the 8^1S_0 level in the same manner described above. Unfortunately, the two lifetime measurements for this level (Table 1) are not in good agreement. We have used the arithmetic average of these two values in calculating the A-values given in Table 3 for the 8^1S_0 reference level. But this leaves an uncertainty of ±14% in these A-values due to the uncertainty in the lifetime.

The ratio of the values referenced to the 7^3S_1 level to those for the 8^1S_0 reference is uniformly close to 1.13 over the whole set of lines. These two sets of A-values could be brought into better agreement in either of two ways. The choice of an 8^1S_0 lifetime value of 65.6 ns, very close to the lower measured lifetime, 63.2 ± 4.8 ns, would shift the 8^1S_0 data into very good agreement with 7^3S_1 data. Alternatively, agreement would be achieved by increasing the electron temperature by 4%, from $kT_e = 0.41$ to 0.425 eV, which is well within our error limits. This would produce changes in the values of both the 7^3S_1 and 8^1S_0 columns. Having no compelling reason for choosing either of these ways over the other, we have left the data unmodified. Note that a change in electron temperature would have negligible effect on the residual disagreement between the values measured in the visible with reference to 7^3S_1 and in the i.r. with reference to 7^1S_0, since these two reference levels have about the same energy.

We feel, however, that the u.v. and visible values based on the 7^3S_1 reference are more accurate than the i.r. values. In particular, the 577 and 579 nm values from the i.r. spectra are based on measurements in the second order of the grating for which the response-function corrections are more uncertain. The estimated uncertainties in our reported A-values are given in a separate column of Table 3. In addition to the large errors given by eqn (12), which have been discussed above, we have also included the statistical errors involved in the measurement of the intensities of both the unknown and the reference lines and uncertainties in the self-absorption corrections. For comparison, we have also listed the values of gA products reported in previous papers. In almost all cases, these values agree with those we are reporting within a factor of ~ 3. More typically, agreement is within a factor of ~ 1.6 in the visible and u.v. region. The data of Ref. (4), as published, differ from other reported values by as much as a factor of 57. Furthermore, the renormalization of these data to yield the correct 7^3S_1 lifetime (see Table 2) still leaves large discrepancies (factors of 8 to 60 relative to other reported data) for lines not originating on 7^3S_1 or 7^1S_0 levels. For this reason, we have included in Table 3 from Ref. (4) only the renormalized values of gA for the four transitions originating on the 7^3S_1 and 7^1S_0 levels.

4. CONCLUSION

A study of the high-pressure mercury positive column at moderate currents has enabled us to establish that the atomic levels are in collisional equilibrium at the electron temperature. This condition, which extends all the way from the continuum to the ground state, allows us to extract transition probabilities from our spectral data. The discharge conditions are such that a rich neutral atomic spectrum is produced while practically no ion spectrum is excited. We include a table giving transition probabilities for 70 lines in the Hg(I) spectrum, many of which have not previously been reported in the literature.

Acknowledgements—The authors would like to thank Dr. K. WALLENSTEIN for making his results available to us prior to publication and Dr. JOHN COOPER for helpful discussion and criticism.

REFERENCES

1. P. JEAN, M. MARTIN, J.-P. BARRAT and J.-L. COJAN, *C. R. Acad. Sci. Paris* **264B**, 1709 (1967).
2. W. PILZ and J. SEEHAWER, *Proc. of 12th Conf. on Phen. in Ion. Gases*, Eindhoven, Part 1, p. 146, North-Holland, Amsterdam (1975).
3. P. PLATZ, *J. de Physique* **32**, 773 (1971).
4. C. H. CORLISS and W. R. BOZMAN, *NBS Monograph* 53 (1962).
5. P. F. GRUZDEV, *Opt. Spectrosc.* **21**, 89 (1967).
6. R. J. ANDERSON, E. T. P. LEE and C. C. LIN, *Phys. Rev.* **159**, 31 (1967).
7. E. R. MOSBURG, JR. and M. D. WILKE, *J. Chem. Phys.* **66**, 5682 (1977).
8. C. CAMHY-VAL, A. M. DUMONT, M. DREUX and R. VITRY, *Phys. Lett.* **32A**, 233 (1970).
9. R. A. HOLT and F. M. PIPKIN, *Phys. Rev.* **9**, 581 (1974).
10. G. C. KING, A. ADAMS and D. CVEJANOVIC, *J. Phys. B* **8**, 365 (1975).
11. R. WALLENSTEIN, Private communication.
12. R. E. DRULLINGER, M. M. HESSEL and E. W. SMITH, *NBS Monograph* 143 (1965).
13. R. E. DRULLINGER, M. M. HESSEL and E. W. SMITH, *J. Chem. Phys.* **66**, 5656 (1977).

APPENDIX

The self-absorption coefficient, A_s, is defined as one minus the ratio of the light received at the detector from a particular atomic transition, to the light which would be received in the absence of atomic self-absorption. The expression relating A_s to the density profiles of upper and lower levels of the transition, $N_u(y)$ and $N_l(y)$, is obtained using eqns (1)–(3). Thus,

$$1 - A_S = I_\lambda / I_{\lambda 0} = \int_{-\infty}^{+\infty} N_u(y) \left[\int_{-\infty}^{+\infty} \alpha(\nu) \exp(-\beta(\nu)\sigma \int_y^{\infty} N_l(y)\mathrm{d}y)\mathrm{d}\nu \right] \mathrm{d}y \Big/ \int_{-\infty}^{+\infty} N_u(y)\,\mathrm{d}y. \tag{A1}$$

We now proceed to relate A_s to the fractional absorption, A_F, measured by the two-source method as described in Section 2. In this method, the light radiated by tube No. 1 is considered as a source and the fraction of this light which is subsequently absorbed in tranversing tube No. 2 is the quantity A_F. Since, in this case, the source lies outside the absorption region of interest, the integral of $N_l(y)$ extends from $-\infty$ to $+\infty$ and the integrals over $N_l(y)$ and $N_u(y)$ are decoupled. The equation for A_F corresponding to eqn (A1) is then

$$1 - A_F = \int_{-\infty}^{+\infty} \alpha(\nu) \exp(-\beta(\nu)\sigma \int_{-\infty}^{+\infty} N_l(y)\mathrm{d}y)\mathrm{d}\nu. \tag{A2}$$

Both tubes are operated under identical conditions so that the emission and absorption spectral profiles are the same. Since the central region of the spacial density distributions, where most of the emission and absorption will occur, can be well fit by a gaussian distribution, we now write

$$N_l(y) = N_l(0) \exp(-t^2) \text{ and } N_u(y) = N_u(0) \exp(-\rho^2 t^2) \tag{A3}$$

where $t \equiv 2\sqrt{(\ln 2)}\, y/\Delta_l$, $\rho \equiv \Delta_l/\Delta_u$, and $\Delta_{l,u}$ are the spacial widths (FWHM) for the lower and upper levels, respectively. We now evaluate the integral over $N_l(y)$ of eqn (A2) and define a new coefficient, K, obtaining

$$\sigma \int_y^{+\infty} N_l(y)\,\mathrm{d}y = \sigma \frac{\Delta_l}{2} \sqrt{\left(\frac{\pi}{\ln 2}\right)} N_l(0) \equiv K. \tag{A4}$$

The similar integral in eqn (A1) can be expressed in terms of the error function and the same coefficient K in the form

$$\sigma \int_y^{+\infty} N_l(y)\mathrm{d}y = \frac{K}{2}[1 - \mathrm{erf}(t)] \tag{A5}$$

Using eqn (A5) in eqn (A1) and expanding the exponential in power series, we obtain for the self-absorption

$$A_S = \sum_{n=1}^{\infty} (-1)^{n+1} \left(\frac{K}{2}\right)^n \frac{1}{n!} C(n)\, I(n), \tag{A6}$$

Table A1. Values of A_S/A_F as a function of A_F for various spectral line profiles.

A_F	Square Profile	Gaussian Profile	Lorentzian Profile	
	$\rho = 1$	$\rho = 1$	$\rho = 1$	$\rho = 1.5$
0	0.500	0.500	0.500	0.500
0.10	0.509	0.510	0.513	0.516
0.20	0.519	0.522	0.529	0.535
0.30	0.530	0.535	0.548	0.557
0.40	0.542	0.550	0.570	0.584
0.50	0.557	0.568	0.599	0.619
0.60	0.575	0.591	0.638	0.665
0.70	0.598	0.621	0.695	0.731
0.80	0.629	0.663	0.782	
0.90	0.677	0.737		

where

$$C(n) \equiv \int_{-\infty}^{+\infty} \alpha(\nu)\beta^n(\nu)\mathrm{d}\nu \tag{A7}$$

and

$$I(n) = \frac{\rho}{\sqrt{\pi}} \int_{-\infty}^{+\infty} \exp(-\rho^2 t^2)[1 - \mathrm{erf}(t)]^n \mathrm{d}t. \tag{A8}$$

For $\rho = 1$, eqn (A8) is expressible in closed form as $I(n) = 2^n/(n+1)$. The spectral line-shape integrals, $C(n)$, for square, Lorentzian and Doppler profiles (absorption and emission profiles identical in each case) are given, respectively, by

$$\left.\begin{aligned} &C(n) = 1, \\ &C(n) = \frac{1}{2}\frac{3}{4}\frac{5}{6}\cdots\cdots\frac{2n-1}{2n}, \\ &\text{and} \\ &C(n) = 1/(n+1). \end{aligned}\right\} \tag{A9}$$

For the fractional absorption, A_F, a similar expansion of the exponential in eqn (A2), using eqn (A4), results in the equation

$$A_F = \sum_{n=1}^{\infty} (-1)^{n+1} K^n \frac{1}{n!} C(n). \tag{A10}$$

By using eqns (A6) and (A10), the relation between A_F and A_S can be established. In Table A1, the ratio A_S/A_F is given vs A_F for $\rho \equiv \Delta_g/\Delta_a = 1$ for the three different profiles mentioned above and for $\rho = 1.5$ in the case of a Lorentzian profile.

As expected, the limiting relation for small absorptions is $A_S \approx 1/2\, A_F$ in all cases but, even for $A_F \approx 0.5$ (approximately the largest absorption encountered in this experiment), the values of A_S/A_F do not differ by more than about 20% from 1/2. The results are rather insensitive to the particular spectral profile and also to the value of ρ.